Synergistic effect of carboxyl and sulfate groups for effective removal of radioactive strontium ion in a Zr-metal-organic framework

Lin Ren, Xudong Zhao, Baosheng Liu and Hongliang Huang

ABSTRACT

Rapid removal of radioactive strontium from nuclear wastewater is of great significance for environmental safety and human health. This work reports the effective adsorption of strontium ion in a stable dual-group metal-organic framework, $Zr_6(OH)_{14}$(BDC-$(COOH)_2)_4(SO_4)_{0.75}$ (Zr-BDC-COOH-SO_4), which contains strontium-chelating groups (-COOH and SO_4) and a strongly ionizable group (-COOH). Zr-BDC-COOH-SO_4 exhibits very rapid adsorption kinetics (<5 min) and a maximum adsorption capacity of 67.5 mg g^{-1}. The adsorption behaviors can be well fitted to the pseudo-second-order model and the Langmuir isotherm model. Further investigations indicate that the adsorption of Sr^{2+} onto Zr-BDC-COOH-SO_4 would not be obviously affected by solution pH and adsorption temperature. The feasible regeneration of the adsorbent was also demonstrated using a simple elution method. Mechanism investigation suggests that free -COOH contributes to the rapid adsorption based on electrostatic interaction, while the introduction of -SO_4 significantly enhanced the adsorption capacity. Thus, these results suggest that Zr-BDC-COOH-SO_4 is a potential candidate for Sr^{2+} removal. They also introduce dual groups as an effective strategy for designing high-efficiency adsorbents.

Key words | adsorption, dual groups, electrostatic interaction, metal-organic framework, radioactive Sr^{2+}

Lin Ren
Department of Chemistry and Chemical Engineering,
LuLiang University,
Lishi 033001,
China

Xudong Zhao (corresponding author)
College of Chemical and Biological Engineering,
Taiyuan University of Science and Technology,
Taiyuan, 030024,
China
E-mail: *zhaoxd@tyust.edu.cn*

Baosheng Liu
College of Materials Science and Engineering,
Engineering Research Center for Magnesium Alloys of Shanxi Province,
Taiyuan University of Science and Technology,
Taiyuan 030024,
China

Hongliang Huang
State Key Laboratory of Separation Membranes and Membrane Processes, School of Chemistry and Chemical Engineering,
Tiangong University,
Tianjin 300387,
China

HIGHLIGHTS

- A dual-group (-COOH and -SO_4) metal-organic framework was used to adsorb radioactive Sr^{2+}.
- Very rapid adsorption kinetics of <5 min was obtained for the adsorbent.
- Large numbers of free carboxyl groups contribute to the fast adsorption.
- Introduction of -SO_4 significantly enhances the adsorption capacity.
- The adsorbent exhibits a good anti-interference ability in terms of temperature and pH.

doi: 10.2166/wst.2021.103

GRAPHICAL ABSTRACT

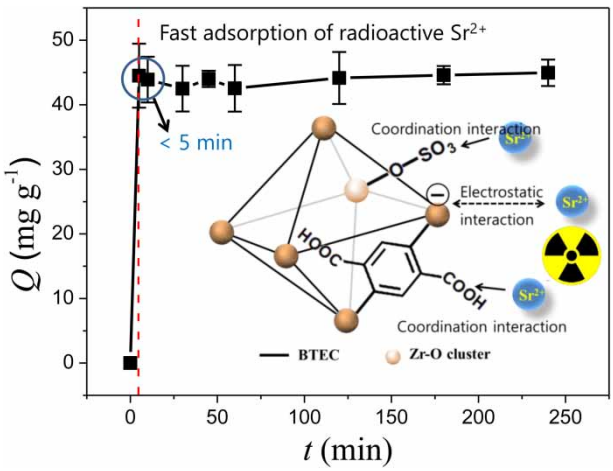

INTRODUCTION

Nuclear power has been widely used for its high efficiency, but every year it produces a large volume of wastewater containing radioactive ions. Among the nuclides, strontium-90 (^{90}Sr) is one of the species of greatest concern for its long half-life ($t_{1/2}$ ~28 years) (Wang *et al.* 2020a). Intake of this radionuclide, even a very low amount, will cause primary harm to the human body (Sachse *et al.* 2012). In addition, $^{90}Sr^{2+}$ as a beta-emitter can also destroy seawater organisms. Thus, removal from aqueous solution is becoming an important technological requirement.

The removal of Sr^{2+} from aqueous systems has been carried out using many common liquid-phase removal methods, including ion exchange, solvent extraction, and adsorption (Roane *et al.* 2003; Marinin & Brown 2000; Rahman *et al.* 2011; Xu *et al.* 2012). Adsorption has attracted a large amount of interest for its low operation cost and high removal efficiency, especially for low concentrations. Consequently, exploring effective adsorbents for $^{90}Sr^{2+}$ would be greatly beneficial for the removal of Sr^{2+}. The reported adsorbents involve carbon-based materials (Qi *et al.* 2015; Song *et al.* 2015), phosphates (Ivanets *et al.* 2020), metal oxides (Zhang *et al.* 2015a; Hong *et al.* 2017), and zeolite (Merceille *et al.* 2012), etc. However, the adsorption efficiency still needs to be greatly improved.

Over the past decade, metal-organic frameworks (MOFs) have emerged as a potential class of functional materials in various applications due to their excellent porosity and designable chemical property (Bavykina *et al.* 2020; Gan *et al.* 2020; Qian *et al.* 2020; Yang *et al.* 2020). Some of the MOFs have proved highly stable in water (Wang *et al.* 2016; Yuan *et al.* 2018; Wang *et al.* 2019; Wang *et al.* 2020b), thus serving as water-phase adsorbents.

For radioactive nuclides, a critical index in adsorbent evaluation is the adsorption kinetics, along with adsorption capacity. The total process of solid-liquid adsorption commonly consists of the diffusion of the guest ion from the liquid system to the surface followed by diffusion into the pores of the adsorbent, and the chemical binding by the adsorption sites. To speed up the adsorption, an effective approach is to improve the diffusion kinetics by introducing a strong interaction between the guest ion and the adsorbent, where electrostatic interaction was a recent focus. In previous reports, several ionizable groups such as -SO_3H (Aguila *et al.* 2016) and -COOH (Mu *et al.* 2019) were integrated into MOFs to enhance the adsorption of Sr^{2+}. However, along with the adsorption process, the host-guest interactions, especially for electrostatic interaction, were gradually weakened due to the coordination of the ionizable groups (e.g. -COOH, -SO_3H) with the ions, leading to the slowing of diffusion kinetics. Thus, a reasonable functionalization for MOFs is needed to maintain a strong electrostatic interaction in the full adsorption process.

In this study, we put forward a dual-group strategy, where one of the groups is responsible for the continuous

electrostatic interaction. For this purpose, a stable Zr-MOF (Zr-BDC-COOH-SO_4) containing benzenedicarboxylate and -COOH and -SO_4 groups was introduced. The free COOH is derived from the organic ligand and -SO_4 is anchored to the Zr-O cluster of the MOF. Although both the -SO_4 and -COOH may be capable of binding Sr, the high density of -COOH can still contribute continuously to negatively charging the surface of the MOF (-COOH $\rightarrow$ -$COO^- + H^+$). The pore and surface of the MOF were characterized and its application for Sr^{2+} adsorption was studied systematically in terms of adsorption isotherm, kinetics, thermodynamics, and effect of pH. The adsorption mechanism as well as the contribution of the two types of groups was also investigated.

MATERIALS AND METHODS

Materials

The chemicals zirconium sulfate hydrate ($Zr(SO_4)_2{\cdot}4H_2O$), 1,2,4,5-benzenetetracarboxylic acid (H_4BTEC), and strontium nitrate ($Sr(NO_3)_2$) were purchased commercially from HWRK Chem. Co. Ltd. All the chemicals were used directly without further purification.

Preparation of adsorbents

The Zr-MOF-COOH-SO_4 was synthesized according to a previous work (Reinsch *et al.* 2015). In a 100 mL round-bottom flask, H_4BTEC (3.8 g, 13.4 mmol) and $Zr(SO_4)_2{\cdot}4H_2O$ (7.1 g, 20 mmol) were mixed in deionized water (40 mL), and then sulfuric acid (2 mL) was added drop-wise into the suspension. The mixture was heated at 90 °C for 16 hours in an oil bath with a refluxing system. After being cooled to room temperature, the resulting solid was collected via filtration and further washed several times with water and acetone. Then the dried solid was treated with 3 vol% H_2SO_4 solution at 60 °C for 12 hours. Finally, the collected solid was again washed with water and acetone, and further dried at 100 °C for 24 hours.

Characterization of materials

The powder X-ray diffraction (PXRD) patterns of the MOFs were recorded on a D8 Advance X diffractometer equipped with Cu Kα radiation ($\lambda = 1.54178$ Å) at room temperature. The 2θ range from 5° to 50° was scanned with a step size of 0.02°. The Brunauer-Emmett-Teller (BET) specific surface area was characterized on an ASAP 2020 surface area analyzer (Micromeritics). The morphology of the sample was characterized using a SU8020 field emission scanning electron microscope (FE-SEM) and a JEM-F200 transmission electron microscope (TEM). Infrared spectra of the samples were recorded on a Nicolet iS50 FTIR spectrophotometer. The zeta potentials at various pH values were measured on a Zetasizer Nano ZS zeta potential analyzer. X-ray photoelectron spectroscopy (XPS) data was collected on an ESCALAB 250 X-ray photoelectron spectroscopy, using Al Kα X-ray as the excitation source.

Adsorption experiments

Non-radioactive Sr^{2+} was used in all of the experiments. In the batch adsorption process, a Zr-MOF-COOH-SO_4 sample (5 mg) was added to Sr^{2+} aqueous solution (10 mL) and the resulting suspension was stirred at a speed of 155 rpm in a constant temperature shaker. After that, the clear filtrate was collected via a microfiltration membrane (0.22 μm) and further used to determine the concentration of Sr^{2+} on a inductively coupled plasma optical emission spectrometer (ICP-OES, Avio 500, PerkinElmer). The adsorption amount was calculated as follows:

$$Q = \frac{(C_0 - C_e) \times V}{m} \quad (1)$$

where C_0 (mg L^{-1}) and C_e (mg L^{-1}) are the initial and final concentrations of Sr^{2+} respectively, V (L) is the volume of Sr^{2+} aqueous solution, m (g) is the mass of the MOF, and Q (mg g^{-1}) is the adsorption amount for Sr^{2+}.

RESULTS AND DISCUSSION

Characterization results

The synthesized MOF was characterized by XRD pattern, N_2 adsorption-desorption isotherms, Fourier transform infrared (FTIR) spectra, XPS pattern, SEM and TEM images. The XRD patterns of the synthesized material are shown in Figure 1(a). To verify the successful synthesis of the material, the standard diffraction data was collected based on the crystal document (.cif) on Materials Studio software. It can be seen that the main diffraction peaks corresponding to the lattice planes (101), (110), (002), (112), (200), (211), (220) of the simulated pattern can be almost found in the powder XRD pattern of this MOF. These measured characteristic diffraction peaks are also consistent with those from the

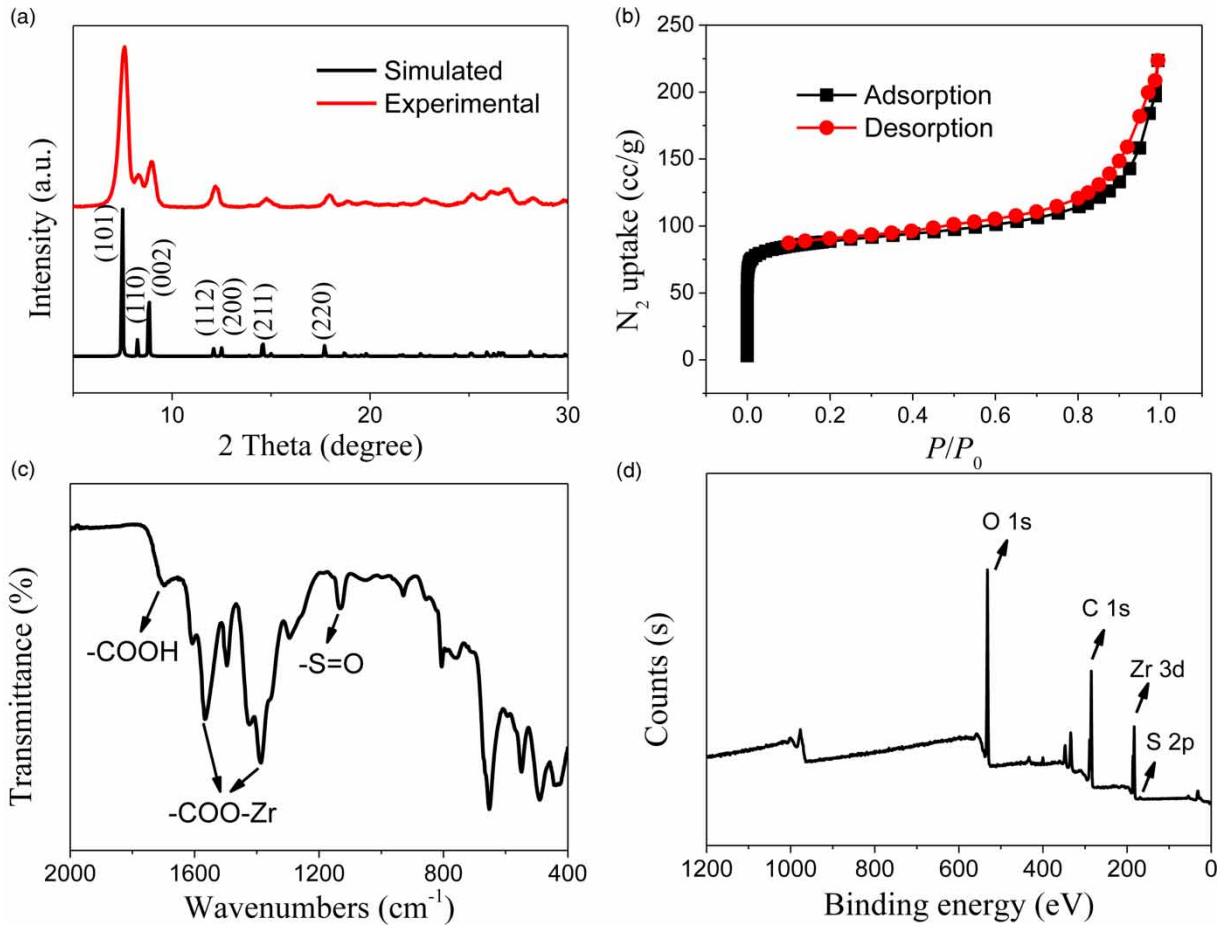

Figure 1 | Characterization results of Zr-MOF-COOH-SO_4: (a) powder XRD patterns and simulated XRD patterns; (b) N_2 adsorption-desorption isotherms at 77 K; (c) FTIR spectrum; (d) XPS pattern.

experimental data in the literature (Reinsch *et al.* 2015). Further, a refinement for the diffraction data was performed. The cell parameters of the MOF were found to be a = b = 14.0946 Å, c = 21.5662 Å and $\alpha = \beta = \gamma = 90°$, almost consistent with the values from the literature (a = b = 14.1669 Å, c = 21.4206 Å and $\alpha = \beta = \gamma = 90°$) (Reinsch *et al.* 2015). These results validate the successful preparation of this Zr-MOF.

The permanent porosity was evaluated by N_2 adsorption-desorption isotherms at 77 K, as shown in Figure 1(b). The BET specific surface area was calculated as 291.42 $m^2\ g^{-1}$, slightly higher than that Reinsch *et al.* (2015) (250 $m^2\ g^{-1}$). This improvement may be attributed to the better activation treatment.

In the FTIR spectrum (Figure 1(c)), the peaks at 1,386.6 cm^{-1} and 1,566.9 cm^{-1} are attributed to the symmetric and asymmetric stretching vibrations of OCO (or -COO-Zr), respectively. The peak at 1,131.5 cm^{-1} is assigned to the vibration of the S = O bond of the SO_4 group and the peak at 1,698.4 cm^{-1} is attributed to the free -COOH in the organic ligand (Li *et al.* 2014; Zhao *et al.* 2016). Hence the existence of -SO_4 and -COOH groups in the MOF can be verified.

The composition of this MOF was determined by element content analysis using XPS (Figure 1(d)). It was found that the atomic ratio of Zr and S was 6:0.75, that is, one Zr_6-inorganic cluster contained 0.75 of an SO_4 group. So the formula of the MOF can be determined to be $Zr_6(OH)_{14}(BTEC)_4(SO_4)_{0.75}$. The -COOH and -$SO_4$ contents were calculated to be ~4.0 and ~0.4 mmol g^{-1} (Zr-MOF).

Finally, the morphology of the material was observed via SEM and TEM images. From Figure 2(a) and 2(b), it can be seen that Zr-MOF-COOH-SO_4 is composed of octahedral particles with a homogenous size of ~100 nm. For a comparison, we further calculated the particle diameter based on the XRD data. The full width half maximum (FWHM) was first determined and then the particle size was

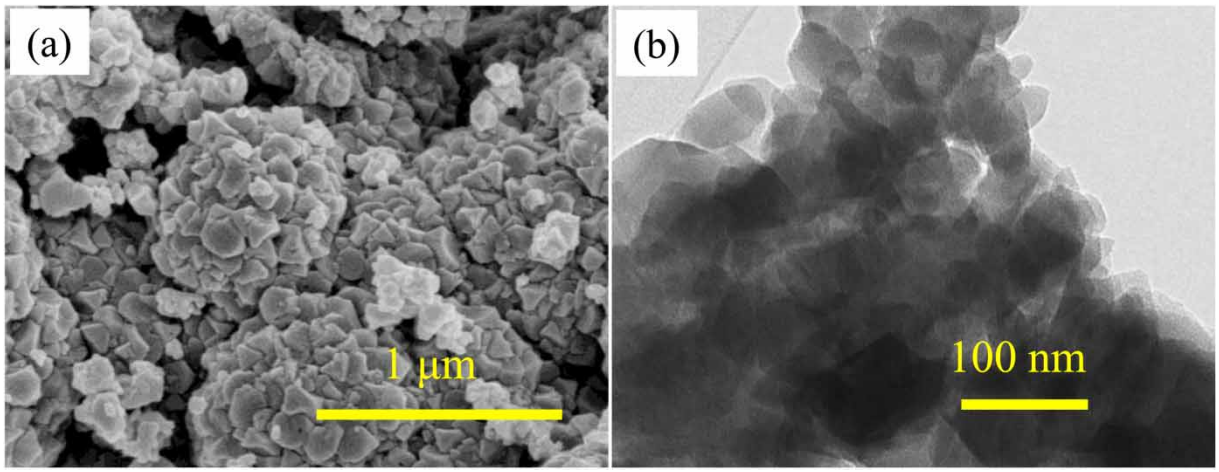

Figure 2 | (a) SEM and (b) TEM images for Zr-MOF-COOH-SO_4.

calculated according to the Scherrer equation. The average value for the peaks centered at 7.5° and 12.1° was found to be 94.73 nm, consistent with the experimental results. So Zr-MOF-COOH-SO_4 exhibits some features such as good porosity, nanoscale size and abundant functional groups, giving it potential for the removal of cationic Sr^{2+} from aqueous solution.

Adsorption of Sr^{2+}

Adsorption kinetics

Adsorption kinetics is an important parameter to evaluate the adsorption performance of adsorbents. It may be controlled by the surface and pore properties of adsorbents, and the detailed characteristics of adsorbates. In particular, the adsorption time is especially important for radioactive $^{90}Sr^{2+}$ to avoid its widespread diffusion in environment. Hence the adsorption amount of Zr-MOF-COOH-SO_4 versus adsorption time was first investigated. As shown in Figure 3, fast and saturated adsorption occurred at only 5 min, indicating that radioactive $^{90}Sr^{2+}$ can be removed quickly by this Zr-MOF.

Further, the adsorption data was fitted to several kinetics models to study the adsorption behavior of Sr^{2+} in Zr-BDC-COOH-SO_4. Three classical isotherms, the pseudo-first-order model, the pseudo-second-order model, and the Weber and Morris intraparticle diffusion model, were used.

The pseudo-first-order model (Lagergren 1898):

$$\ln(Q_e - Q_t) = \ln Q_e - k_1 t \tag{2}$$

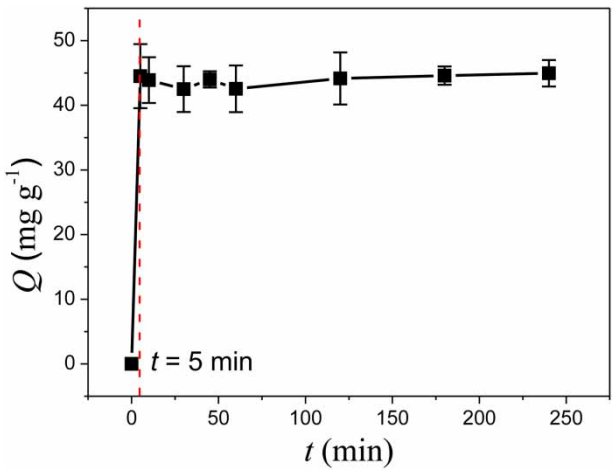

Figure 3 | Adsorption amount of Sr^{2+} versus time (conditions: C_0, 100 mg L^{-1}; T, 303 K; natural (unmodified) pH).

The pseudo-second-order model (Zhao *et al.* 2014):

$$\frac{t}{Q_t} = \frac{1}{k_2 Q_e^2} + \frac{t}{Q_e} \tag{3}$$

The Weber and Morris intraparticle diffusion model (Weber & Morris 1963):

$$Q_t = k_{id} t^{0.5} + C \tag{4}$$

where Q_e (mg g^{-1}) is the equilibrium adsorption capacity for Sr^{2+}, Q_t (mg g^{-1}) is the adsorption capacity for Sr^{2+} at time t (min), k_1 (min^{-1}), k_2 (g min^{-1} mg^{-1}), and k_{id} (mg g^{-1} $min^{-0.5}$) are the rate constants of the pseudo-first order model, the pseudo-second-order model, and the intraparticle

diffusion model, respectively. From the fitting parameters (Table 1) especially the correlation coefficient R^2, the adsorption behavior of Sr^{2+} onto Zr-MOF-COOH-SO_4 can be well described by pseudo-second-order model. This indicates that the rate-controlling step of the adsorption process is chemical adsorption.

Adsorption isotherm and thermodynamics

The adsorption capacity of Zr-MOF-COOH-SO_4 was investigated based on the adsorption isotherms at the initial concentration range of 10–500 mg L^{-1}. Figure 4(a) lists three adsorption isotherms at 293, 303, and 313 K, respectively. It can be seen that the adsorption capacity decreases slightly with the increase in adsorption temperature. The maximum adsorption capacities were found to be 71.6, 67.5, and 64.5 mg g^{-1} at 293, 303, and 313 K, respectively. This indicates that room temperature rather than higher temperatures enable efficient removal of Sr^{2+}. As a comparison, the adsorption performances of other reported Sr^{2+} adsorbents were investigated (İnan & Altaş 2010, 2011; Tel *et al.* 2010; Wu *et al.* 2012; Song *et al.* 2015; Tayyebi *et al.* 2015; Zhang *et al.* 2015a, 2015b; Xiao *et al.* 2016; Asgari *et al.* 2019; Mu *et al.* 2019; El-saied *et al.* 2020). As listed in Table 2, Zr-MOF-COOH-SO_4 exhibits a superior adsorption capacity compared to other adsorbents including metal oxides, GO-type materials, and some modified minerals. Although the capacities of KTN_{flux}-600 and MOF-808-SO_4 (or -C_2O_4) are higher than that of Zr-MOF-COOH-SO_4, the adsorption equilibrium time of those materials (2 or 3 hours) is considerably longer than the 5 min of this work. Thus, we suggest the material in this work may be a promising adsorbent for Sr^{2+}.

The adsorption mode of Sr^{2+} onto Zr-MOF-SO_4/COOH was studied through the fitting to several isotherms models.

The Langmuir isotherm model (Langmuir 1916):

$$\frac{C_e}{Q_e} = \frac{1}{bQ_m} + \frac{C_e}{Q_m} \tag{5}$$

The Freundlich isotherm model (Freundlich 1906):

$$\ln Q_e = lnK_F + \frac{1}{n} lnC_e \tag{6}$$

where C_e (mg L^{-1}) is the equilibrium concentration of Sr^{2+}, b (L mg^{-1}) and Q_m (mg g^{-1}) are the Langmuir constant and Langmuir adsorption capacity, respectively; n and K_F [(L $mg^{-1})^{1/n}$ mg g^{-1}] are related to the adsorption intensity and capacity, respectively. From the values of Q_m and the correlation coefficient R^2 (Table 3), the adsorption behavior agrees better with the Langmuir model than the Freundlich model, validating the homogenous distribution of adsorption sites and the monolayer adsorption of Sr^{2+} onto Zr-BDC-COOH-SO_4.

Table 1 | Kinetics model parameters of Sr^{2+} adsorbed onto Zr-MOF-COOH-SO_4

Model	Modelling parameters	Value
Pseudo-first-order	$Q_{e.cal}$ (mg g^{-1})	1.8371
	k_1 (min^{-1})	0.0111
	R^2	0.5855
Pseudo-second-order	$Q_{e.cal}$ (mg g^{-1})	45.05
	k_2 (g min^{-1} mg^{-1})	0.0169
	R^2	0.9998
Intraparticle diffusion	k_{id} (mg g^{-1} $min^{-0.5}$)	0.0793
	C	43.25
	R^2	0.1727

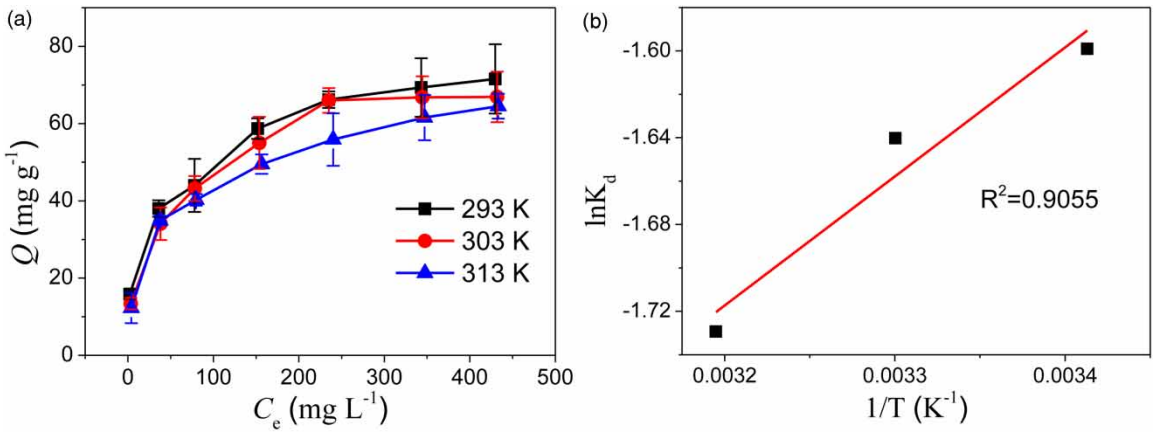

Figure 4 | (a) Adsorption isotherms at different temperatures (conditions: natural pH; t, 12 hours); (b) van 't Hoff plot of Sr^{2+} adsorption onto Zr-MOF-COOH-SO_4.

Table 2 | Comparison of maximum adsorption capacities of adsorbents

Adsorbents	Q_{max} (mg g^{-1})	Equilibrium time (min)	Temperature (K)	Reference
Wet-oxidized OMC FDU-15	7.3	5	298	Song *et al.* (2015)
ZrO_2	10.5[a]	150	303	Tel *et al.* (2010)
Ca-Mt	13.2	~1,500	301	Wu *et al.* (2012)
M-GO	14.3	300	R.T.	Tayyebi *et al.* (2015)
Zn-Mn oxide/PAN	21.4		333	İnan & Altaş (2011)
Sb(III)/Sb_2O_5	23.6[a]	~6	303	Zhang *et al.* (2015a)
Zr-Mn oxide	30.9	~165	303	İnan & Altaş (2010)
SANCHs nanocomposite	47.2	180	R.T.	El-saied *et al.* (2020)
SiSb-1	~55	~30	303	Zhang *et al.* (2015b)
Nd-BTC	58	~60	298	Asgari *et al.* (2019)
APTES-Mt	65.6	~3,000	301	Wu *et al.* (2012)
Zr-MOF-SO_4/COOH	67.5	5	303	This work
KTN_{flux}-600	91.1	180	R.T.	Xiao *et al.* (2016)
MOF-808-SO_4	176.6	120	293	Mu *et al.* (2019)
MOF-808-C_2O_4	206.3	120	293	Mu *et al.* (2019)

[a]The values were obtained from the Langmuir model fitting result.

Table 3 | Isotherms models parameter of Sr^{2+} adsorbed onto Zr-MOF-COOH-SO_4

Adsorption model	Modelling parameter	Value		
		293 K	303 K	313 K
Langmuir	$Q_{m,1}$ (mg g^{-1})	76.34	73.53	68.49
	b (L mg^{-1})	0.0287	0.0247	0.0238
	R^2	0.9954	0.9946	0.9905
Freundlich	k_F [(mg g^{-1})(L $mg^{-1})^{1/n}$]	12.85	7.129	8.365
	$1/n$	0.2922	0.3945	0.3484
	R^2	0.9934	0.9698	0.9764

The thermodynamic behavior of Sr^{2+} adsorption onto Zr-MOF-COOH-SO_4 was studied. The thermodynamic parameters standard enthalpy change (ΔH°), entropy change (ΔS°), and Gibbs energy change (ΔG°) were calculated according to the thermodynamic equations:

$$K_d = \frac{Q_e}{C_e} \tag{7}$$

$$\ln K_d = \frac{\Delta S^\circ}{R} - \frac{\Delta H^\circ}{RT} \tag{8}$$

$$\Delta G^\circ = \Delta H^\circ - T\Delta S^\circ \tag{9}$$

where K_d (L g^{-1}) is the adsorption equilibrium constant and R is the universal constant. The relationship of $\ln K_d$ and $1/T$ at $C_0 = 400$ mg L^{-1} is illustrated in Figure 4(b); the parameters were calculated according to the fitting results. The negative values of ΔS° (−30.1 J mol^{-1} K^{-1}) and ΔH° (−4.9 kJ mol^{-1}) indicate the adsorption process is an entropy decrease reaction and beneficial from the enthalpy decrease effect. The ΔG° at 293, 303, and 313 K were determined as the positive values of 3.9, 4.2, and 4.5 kJ mol^{-1}, caused by the low values of K_d (Q_e/C_e). This is attributed to the fact that the small pore channels of the material may limit the full use of the interior adsorption sites and thereby the much larger capacity, due to the pore blockage effect. As a comparison, ΔG° was found to have a negative value at the lower concentration where the adsorption percentage of Sr^{2+} was larger and thereby the K_d value was significantly enhanced. As proved in the 'Adsorption kinetics' and 'Adsorption mechanism' sections, this adsorption process involves a strongly chemical reaction. Thus, even with the positive values, the adsorption of Sr^{2+} onto Zr-MOF-COOH-SO_4 is still practicable due to the strong host-guest chemical interactions.

Effect of solution pH

Adsorption of ionic adsorbates is commonly controlled by solution pH, which determines the surface charge property of adsorbents and detailed existing mode of adsorbates. Therefore, the effect of pH on the adsorption as well as

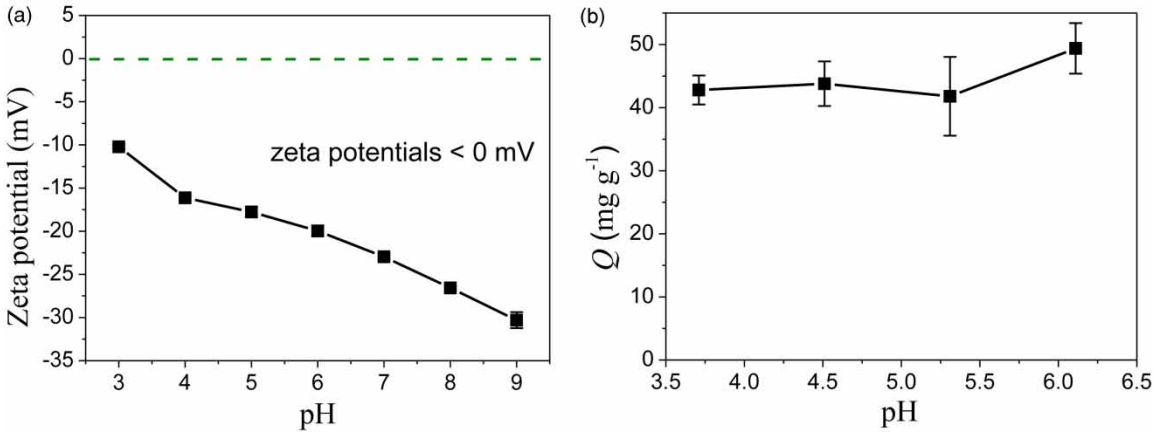

Figure 5 | (a) Zeta potentials of Zr-BDC-COOH-SO_4 at a pH range of 3.0–9.0; (b) adsorption capacity at a pH range of 3.7–6.2 (conditions: C_0, 100 mg L^{-1}; t, 12 hours; T, 303 K).

the optimal pH was investigated. First, the zeta potentials of Zr-MOF-COOH-SO_4 in the pH range of 3.0–9.0 were measured, as shown in Figure 5(a). It can be seen that in the wide pH range, the surface of the material is always negatively charged, attributed to the ionization process of the functional groups, especially for -COOH (MOF-COOH $\rightarrow$ MOF-$COO^- + H^+$). Considering the pH of the Sr^{2+}-containing wastewater is commonly in the acidic range, we studied the adsorption behavior of Zr-BDC-COOH-SO_4 in acidic solutions. The effect of pH on the adsorption behavior is shown in Figure 5(b). In the pH range of 3.7–5.3, the adsorption amount of Sr^{2+} depends slightly on solution pH; while at pH >5.3, the extent of Sr^{2+} adsorption was enhanced, which may be attributed to the enhanced electrostatic interaction between Sr^{2+} and the negatively charged MOF sample.

Regeneration investigation

From the point of view of practical application, an adsorbent should be reusable to control the cost. Therefore, the regeneration of Zr-BDC-COOH-SO_4 was investigated. A two-step washing method using Na_2SO_4 aqueous solution (500 mg L^{-1}) and HNO_3 solution (pH = 2) was used. In detail, an Sr^{2+}-loaded sample was successively immersed in the two solutions and stirred for 12 hours to wash away the adsorbed Sr^{2+}. After that, the sample was slightly washed with deionized water and further dried. As shown in Figure 6, after three uses, the adsorption capacity of the sample could still reach ~70% of that of the fresh sample. This decrease may be attributed to the strong host-guest binding force and the incomplete desorption of Sr^{2+} from the adsorbent. Even so, the capacity after three uses is still

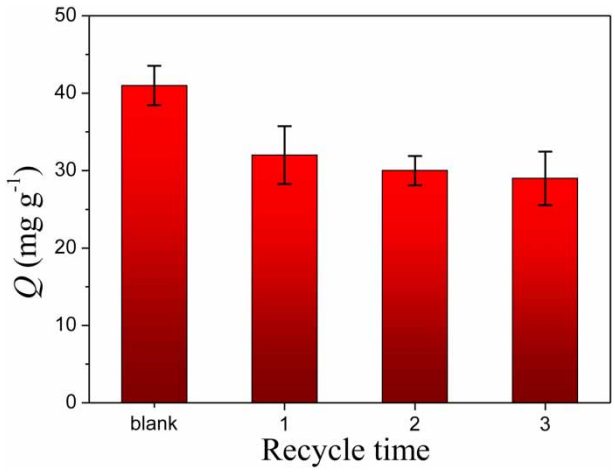

Figure 6 | The reusability of Zr-BDC-COOH-SO_4 using Na_2SO_4 and HNO_3 as the eluents (conditions: natural pH; t, 12 hours; T, 303 K; C_0, 100 mg L^{-1}).

higher than those of materials like Sb(III)/Sb_2O_5 (Zhang *et al.* 2015a) and M-GO (Tayyebi *et al.* 2015).

Adsorption mechanism

First, the adsorption of Sr^{2+} onto Zr-MOF-COOH-SO_4 was confirmed through XPS. As shown in Figure 7(a), the signature of Sr 3d can be clearly found in the XPS pattern of the sample after adsorption, validating the existence of the Sr element in the sample. The powder XRD pattern of the sample after adsorption was also measured. An obvious decrease in the long-range order can be seen in Figure 7(b), which is attributed to the fact that the introduction of Sr^{2+} affects the coordination of the Zr-O cluster and the SO_4^{2-} ion. Meanwhile, the main distinct diffraction peaks remained, indicating that the framework of the MOF remained relatively complete. Similar phenomena can be

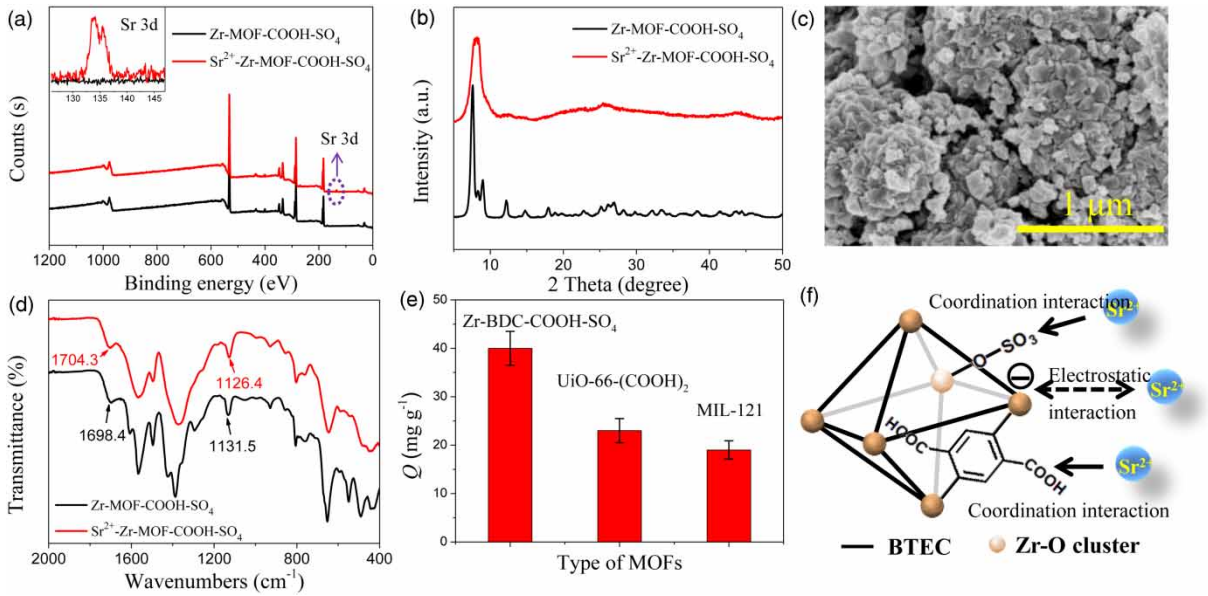

Figure 7 | Mechanism analysis for Sr^{2+} adsorption onto Zr-BDC-COOH-SO_4: (a) XPS patterns; (b) powder XRD patterns; (c) SEM image of Sr^{2+}-loaded sample: (d) FTIR spectra; (e) adsorption capacity of Zr-BDC-COOH-SO_4, UiO-66-$(COOH)_2$, and MIL-121 at $C_0 = 100$ mg L^{-1}; (f) possible adsorption mechanism based on coordination interaction and electrostatic interaction.

found in the high-temperature activation process of this MOF (Reinsch *et al.* 2015). This conclusion can also be verified by the SEM image. As shown in Figure 7(c), compared with the original MOF (Figure 2(a)), there are no obvious changes in either surface or morphology.

The detailed adsorption mechanism was further analyzed by FTIR, as shown in Figure 7(d). After adsorption, the peak assigned to S = O shifted from 1,131.5 cm^{-1} to 1,126.4 cm^{-1} and the sign of free -COOH also showed a change from 1,698.4 cm^{-1} to 1,704.3 cm^{-1}, verifying the binding between Sr^{2+} and -SO_4 and -COOH. Furthermore, the degree of contribution of these groups was evaluated through a comparison with UiO-66-$(COOH)_2$ (Zr-BDC-COOH) and MIL-121 (Al-BDC-COOH). The contents of free -COOH in these MOFs are 5.5 and 6.7 mmol g^{-1} respectively, comparable with that of Zr-BDC-COOH-SO_4 (4.0 mmol g^{-1}). At the same condition (100 mg L^{-1}), the adsorption capacities of the two MOFs were measured as 23.2 and 19.0 mg g^{-1}, lower than that of Zr-BDC-COOH-SO_4 (40.0 mg g^{-1}) (Figure 7(e)). This highlights the important contribution of -SO_4 groups.

FInally, the surface charge property of the Sr^{2+}-loaded sample was analyzed. Zr-BDC-COOH-SO_4 was immersed in the Sr^{2+} solution ($pH_0 = 6.0$, $pH_f = \sim 4.0$) for 12 hours and then the solid was collected and further dried. The zeta potential of the sample at pH = 4.0 was measured as −3.5 mV, indicating the surface of this Zr-MOF was always negatively charged in the total adsorption process. As a result, a strong electrostatic interaction existed in the adsorption process, including the diffusion step of Sr^{2+}, which was the main reason for the rapid kinetics. Therefore, in the Zr-BDC-COOH-SO_4, the high density of -COOH was beneficial for the rapid adsorption and capture of Sr^{2+}, but the introduction of -SO_4 improved the adsorption capacity. The possible adsorption mechanism is illustrated in Figure 7(f).

CONCLUSION

In this work, Zr-BDC-COOH-SO_4 with dual functional groups was introduced for the adsorptive removal of Sr^{2+} from wastewater. Due to the anchored -SO_4 and high density of -COOH groups, the material exhibited an ideal adsorption capacity and very rapid adsorption kinetics. In addition, an excellent lack of sensitivity towards temperature and solution pH was demonstrated. Compared with those MOFs with single type of adsorption site, the dual-group MOF shows a promising application when the surface charge property and active adsorption sites can be well controlled. Therefore, this work not only demonstrates that Zr-BDC-COOH-SO_4 is a potential adsorbent for radioactive Sr^{2+} in nuclear wastewater treatment, but also highlights a

new method for designing adsorbents by introducing dual functional groups.

ACKNOWLEDGEMENTS

This work was supported by Scientific and Technological Innovation Programs of Higher Education Institutions in Shanxi (No. 2019L0960) and LuLiang Key Research and Development Projects (No. GXZDYF2019084).

DATA AVAILABILITY STATEMENT

All relevant data are included in the paper or its Supplementary Information.

REFERENCES

Aguila, B., Banerjee, D., Nie, Z., Shin, Y., Ma, S. & Thallapally, P. K. 2016 Selective removal of cesium and strontium using porous frameworks from high level nuclear waste. *Chemical Communication* **52**, 5940–5942.

Asgari, P., Mousavi, S. H., Aghayan, H., Ghasemi, H. & Yousefi, T. 2019 Nd-BTC metal-organic framework (MOF): synthesis, characterization and investigation on its adsorption behavior toward cesium and strontium ions. *Microchemical Journal* **150**, 104188.

Bavykina, A., Kolobov, N., Khan, I. S., Bau, J. A., Ramirez, A. & Gascon, J. 2020 Metal-organic frameworks in heterogeneous catalysis: recent progress, new trends, and future perspectives. *Chemical Review* **120**, 8468–8535.

El-saied, H.-A., Shahr El-Din, A. M., Masry, B. A. & Ibrahim, A. M. 2020 A promising superadsorbent nanocomposite based on grafting biopolymer/nanomagnetite for capture of ^{134}Cs, ^{85}Sr and ^{60}Co radionuclides. *Journal of Polymers and the Environment* **28**, 1749–1765.

Freundlich, H. M. F. 1906 Über Die adsorption in Lösungen (Adsorption in solution). *Zeitschrift für Physikalische Chemie* **57**, 385–470.

Gan, L., Chidambaram, A., Fonquernie, P. G., Light, M. E., Choquesillo-Lazarte, D., Huang, H., Solano, E., Fraile, J., Viñas, C., Teixidor, F., Navarro, J. A. R., Stylianou, K. C. & Planas, J. G. 2020 A highly water-stable meta-carborane-based copper metal-organic framework for efficient high-temperature butanol separation. *Journal of the American Chemical Society* **142**, 8299–8311.

Hong, H.-J., Kim, B.-G., Hong, J., Ryu, J., Ryu, T., Chung, K.-S., Kim, H. & Park, I.-S. 2017 Enhanced Sr adsorption performance of MnO_2-alginate beads in seawater and evaluation of its mechanism. *Chemical Engineering Journal* **319**, 163–169.

İnan, S. & Altaş, Y. 2010 Adsorption of strontium from acidic waste solution by Mn-Zr mixed hydrous oxide by co-precipitation. *Separation Science and Technology* **45**, 269–276.

İnan, S. & Altaş, Y. 2011 Preparation of zirconium-manganese oxide/polyacrylonitrile (Zr-Mn oxide/PAN) composite spheres and the investigation of Sr(II) sorption by experimental design. *Chemical Engineering Journal* **168**, 1263–1271.

Ivanets, A., Milyutin, V., Shashkova, I., Kitikova, N., Nekrasova, N. & Radkevich, A. 2020 Sorption of stable and radioactive Cs(I), Sr(II), Co(II) ions on Ti-Ca-Mg phosphates. *Journal of Radioanalytical and Nuclear Chemistry* **324**, 1115–1123.

Lagergren, S. 1898 Theorie der Sogenannten Adsorption Geloster Stoffe (Theory of so-called adsorption soluble substances), Kungliga Svenska Veten-skapsakademiens. *Handlingar* **24**, 1–39.

Langmuir, I. 1916 The constitution and fundamental properties of solid and liquids. Part I. Solids. *Journal of the American Chemical Society* **38**, 2221–2295.

Li, B., Zhang, Y., Krishna, R., Yao, K., Han, Y., Wu, Z., Ma, D., Shi, Z., Pham, T., Space, B., Liu, J., Thallapally, P. K., Liu, J., Chrzanowski, M. & Ma, S. 2014 Introduction of π-complexation into porous aromatic framework for highly selective adsorption of ethylene over ethane. *Journal of the American Chemical Society* **136**, 8654–8660.

Marinin, D. V. & Brown, G. N. 2000 Studies of sorbent/ion-exchange materials for the removal of radioactive strontium from liquid radioactive waste and high hardness groundwaters. *Waste Management (Oxford)* **20**, 545–553.

Merceille, A., Weinzaepfel, E., Barre, Y. & Grandjean, A. 2012 The sorption behaviour of synthetic sodium nonatitanate and zeolite A for removing radioactive strontium from aqueous wastes. *Separation and Purification Technology* **96**, 81–88.

Mu, W., Du, S., Li, X., Yu, Q., Hu, R., Wei, H., Yang, Y. & Peng, S. 2019 Efficient and irreversible capture of strontium ions from aqueous solution using metal-organic frameworks with ion trapping groups. *Dalton Transactions* **48**, 3284–3290.

Qi, H., Liu, H. & Gao, Y. 2015 Removal of Sr(II) from aqueous solutions using polyacrylamide modified graphene oxide composites. *Journal of Molecular Liquids* **208**, 394–401.

Qian, Q., Asinger, P. A., Lee, M. J., Han, G., Rodriguez, K. M., Lin, S., Benedetti, F. M., Wu, A. X., Chi, W. S. & Smith, Z. P. 2020 MOF-based membranes for gas separation. *Chemical Review* **120**, 8161–8266.

Rahman, R. O. A., Ibrahim, H. A. & Hung, Y. 2011 Liquid radioactive waste treatment: a review. *Water* **3**, 551–565.

Reinsch, H., Bueken, B., Vermoortele, F., Stassen, I., Lieb, A., Lillerud, K.-P. & De Vos, D. 2015 Green synthesis of zirconium-MOFs. *CrystEngComm* **17**, 4070–4074.

Roane, J. E., Devol, T. A., Leyba, J. D. & Fjeld, R. A. 2003 The use of extraction chromatography resins to concentrate actinides and strontium from soil for radiochromatographic analyses. *Journal of Environmental Radioactivity* **66**, 227–245.

Sachse, A., Merceille, A., Barre, Y., Grandjean, A., Fajula, F. & Galarneau, A. 2012 Macroporous LTA-monoliths for in-flow removal of radioactive strontium from aqueous effluents: application to the case of Fukushima. *Microporous Mesoporous Materials* **164**, 251–258.

Song, Y., Ye, G., Chen, J., Lv, D. & Wang, J. 2015 Wet oxidation of ordered mesoporous carbon FDU-15 by using $(NH_4)_2S_2O_8$ for fast adsorption of Sr(II): an investigation of surface chemistry and adsorption mechanism. *Applied Surface Science* **357**, 1578–1586.

Tayyebi, A., Outokesh, M., Moradi, S. & Doram, A. 2015 Synthesis and characterization of ultrasound assisted 'graphene oxide-magnetite' hybrid, and investigation of its adsorption properties for Sr(II) and Co(II) ions. *Applied Surface Science* **353**, 350–362.

Tel, H., Altaş, Y., Eral, M., Sert, Ş., Çetinkaya, B. & İnan, S. 2010 Preparation of ZrO_2 and ZrO_2-TiO_2 microspheres by the sol-gel method and an experimental design approach to their strontium adsorption behaviours. *Chemical Engineering Journal* **161**, 151–160.

Wang, B., Lv, X.-L., Feng, D., Xie, L.-H., Zhang, J., Li, M., Xie, Y., Li, J.-R. & Zhou, H.-C. 2016 Highly stable Zr(VI)-based metal-organic frameworks for the detection and removal of antibiotics and organic explosives in water. *Journal of the American Chemical Society* **138**, 6204–6216.

Wang, K., Huang, H., Zhou, X., Wang, Q., Li, G., Shen, H., She, Y. & Zhong, C. 2019 Highly chemically stable MOFs with trifluoromethyl groups: effect of position of trifluoromethyl groups on chemical stability. *Inorganic Chemistry* **58**, 5725–5732.

Wang, K.-Y., Sun, M., Ding, D., Liu, H.-W., Cheng, L. & Wang, C. 2020a Di-lacunary $[In_6S_{15}]^{12-}$ cluster: building block of a highly negative charged framework for superior Sr^{2+} adsorption capacities. *Chemical Communication* **56**, 3409–3412.

Wang, K., Wang, Q., Wang, X., Wang, M., Wang, Q., Shen, H.-M., Yang, Y.-F. & She, Y. 2020b Intramolecular hydrogen bond-induced high chemical stability of metal-organic frameworks. *Inorganic Chemistry Frontiers* **7**, 3548–3554.

Weber, W. J. & Morris, J. C. 1963 Kinetics of adsorption on carbon from solution. *Journal of the Sanitary Engineering Division, American Society of Civil Engineers* **89**, 31–40.

Wu, P., Dai, Y., Long, H., Zhu, N., Li, P., Wu, J. & Dang, Z. 2012 Characterization of organo-montmorillonites and comparison for Sr(II) removal: equilibrium and kinetic studies. *Chemical Engineering Journal* **191**, 288–296.

Xiao, X., Hayashi, F., Shiiba, H., Selcuk, S., Ishihara, K., Namiki, K., Shao, L., Nishikiori, H., Selloni, A. & Teshima, K. 2016 Platy $KTiNbO_5$ as a selective Sr ion adsorbent: crystal growth, adsorption experiments, and DFT calculations. *Journal of Physical Chemistry C* **120**, 11984–11992.

Xu, C., Wang, J. & Chen, J. 2012 Solvent extraction of strontium and cesium: a review of recent progress. *Solvent Extraction and Ion Exchange* **30**, 623–650.

Yang, S., Peng, L., Syzgantseva, O. A., Trukhina, O., Kochetygov, I., Justin, A., Sun, D. T., Abedini, H., Syzgantseva, M. A., Oveisi, E., Lu, G. & Queen, W. L. 2020 Preparation of highly porous metal-organic framework beads for metal extraction from liquid streams. *Journal of the American Chemical Society* **142**, 13415–13425.

Yuan, S., Feng, L., Wang, K., Pang, J., Bosch, M., Lollar, C., Sun, Y., Qin, J., Yang, X., Zhang, P., Wang, Q., Zou, L., Zhang, Y., Zhang, L., Fang, Y., Li, J. & Zhou, H.-C. 2018 Stable metal-organic frameworks: design, synthesis, and applications. *Advanced Materials* **30**, 1704303.

Zhang, L., Wei, J., Zhao, X., Li, F., Jiang, F. & Zhang, M. 2015a Strontium(II) adsorption on Sb(III)/Sb_2O_5. *Chemical Engineering Journal* **267**, 245–252.

Zhang, L., Wei, J., Zhao, X., Li, F. & Jiang, F. 2015b Adsorption characteristics of strontium on synthesized antimony silicate. *Chemical Engineering Journal* **277**, 378–387.

Zhao, X., Liu, D., Huang, H., Zhang, W., Yang, Q. & Zhong, C. 2014 The stability and defluoridation performance of MOFs in fluoride solutions. *Microporous Mesoporous Materials* **185**, 72–78.

Zhao, X., Liu, D., Huang, H. & Zhong, C. 2016 Highly selective and sensitive metal-organic framework fluorescent probe for Cu^{2+} through rational design of binding sites. *Microporous Mesoporous Materials* **224**, 149–154.

First received 17 January 2021; accepted in revised form 8 March 2021. Available online 19 March 2021